Research Article Vol. 57, No. 8 / 10 March 2018 / Applied Optics 1883

applied optics

High-sensitivity birefringent and single-layer coating photonic crystal fiber biosensor based on surface plasmon resonance

MIN LIU,[1,2,*] XU YANG,[1,2] PING SHUM,[3] AND HONGTAO YUAN[1,2]

[1]College of Communication Engineering, Chongqing University, Chongqing 400044, China
[2]Key Laboratory of Optoelectronic Technology and Systems (Education Ministry of China), Chongqing University, Chongqing 400044, China
[3]School of Electrical & Electronic Engineering, Nanyang Technological University, Singapore 639798, Singapore
*Corresponding author: liumin@cqu.edu.cn

Received 22 November 2017; revised 1 February 2018; accepted 1 February 2018; posted 2 February 2018 (Doc. ID 314039); published 7 March 2018

A birefringent single-layer coating photonic crystal fiber biosensor based on surface plasmon resonance is proposed to realize high sensitivity, which is easy to implement, in that only gold is deposited externally. The birefringent nature of the structure provides the sensor with high sensitivity. The results show that the biosensor can obtain the wavelength sensitivity of 15180 nm/refractive index unit (RIU) and high linearity with the analyte RI range of 1.40–1.43, corresponding to the resolution of 5.6818×10^{-6} RIU. Owing to the high sensitivity and simple structure, the proposed sensor can find important applications in biochemical and biological analyte detection.

OCIS codes: (060.2370) Fiber optics sensors; (240.6680) Surface plasmons; (060.5295) Photonic crystal fibers; (060.4005) Microstructured fibers.

https://doi.org/10.1364/AO.57.001883

1. INTRODUCTION

As an alternative to bulky configuration, photonic crystal fiber (PCF)-based surface plasmon resonance (SPR) biosensors have attracted significant research attention because of advantages such as miniaturization, integration, etc. [1–4]. It is important to make the selection of plasmonic materials in SPR sensors. With silver (Ag) material, it is possible to obtain a sharp resonance peak to improve the sensing. However, Ag has high susceptibility to oxidization. Although a thin graphene or Ta_2O_5 layer coating can solve the oxidization problem, this additional coating increases the fabrication difficulty [5]. Comparatively, gold (Au) is chemically stable and does not oxidize easily [6]. Moreover, it is more sensitive because of lager resonance peaks.

Different methods have been investigated for better sensing performance. Yang *et al.* reported a SPR biosensor, where a coated graphene–Ag bimetallic layer was used as the analyte channel [7]. Rifat *et al.* have proposed graphene–Ag deposited core-based SPR sensors with selectively filled analyte channels for RI detection [8]. Fan *et al.* reported two kinds of novel refractive index sensors based on PCFs deposited with Au or Ag [9]. Very recently, a pure silica core PCF with Au and Ta_2O_5 layers in the large air holes at the vertical direction for high RI sensing was proposed [10]. These multi-coating and internally metal film-coated SPR sensors have severe drawbacks, because it is difficult to infiltrate the analyte in the inner air holes for practical sensing. To solve the problems, externally coated metallic film SPR sensors have been introduced. A D-shaped RI sensor with a Ag film to obtain SPR has been presented by Luan *et al.* [11]. Liu *et al.* proposed a PCF-SPR sensor with the Au–graphene composite film deposited on the outermost layer of the core region, and the maximum wavelength sensitivity can reach 7500 nm/RIU [12]. With only one plasmonic material, Liu *et al.* presented a square array PCF-based SPR RI sensor with 7250 nm/RIU [13]. It should be noted that easier fabrication and higher sensitivity are important measures of sensor performance.

In this paper, we report a simple SPR-PCF sensor based on a single coating layer in which a thin film of Au exists outside the PCF structure to realize an easy coating process. The air holes for both polarization directions are different to create the birefringence, which allows one fundamental mode to be more sensitive. By optimizing the structure parameters, sensitivity as high as 15180 nm/RIU and resolution as low as 5.6818×10^{-6} RIU can be achieved within the detection RI range of 1.40–1.43 and with high linearity, which is remarkable compared with sensitivity of 9180 nm/RIU in Ref. [10] and 7500 nm/RIU in Ref. [12].

1559-128X/18/081883-04 Journal

2. STRUCTURE DESIGN AND NUMERICAL MODELING

The cross section of the proposed birefringent single-layer coating PCF-SPR biosensor is shown in Fig. 1. The sizes of the air holes are $r_1 = 0.8$ μm, $r_2 = 0.7$ μm, and $r_3 = 0.4$ μm, respectively. The hole spacings are $\Lambda_1 = 1.8$ μm and $\Lambda_2 = \Lambda_3 = 1.5$ μm. The radius of the silica core is $r_c = 3$ μm. The thickness of Au film and analyte channel are $t_{Au} = 30$ nm and $t_{anal} = 0.5$ μm. n_a represents the refractive index of the analyte. The proposed structure can be fabricated by the stack and draw method. The Au film can be deposited on the external surface of the PCF structure through high chemical vapor deposition (CVD) to offer uniform nanolayer coating with minimal surface roughness and high efficiency [5].

The background material of the proposed sensor is fused silica whose material dispersion is considered by the Sellmeier equation [5]:

$$n^2(\lambda) = 1 + \frac{B_1\lambda^2}{\lambda^2 - C_1} + \frac{B_2\lambda^2}{\lambda^2 - C_2} + \frac{B_3\lambda^2}{\lambda^2 - C_3}, \quad (1)$$

where n is the wavelength-dependent refractive index of fused silica, and λ is the input wavelength. B_1, B_2, B_3, C_1, C_2, and C_3 are the Sellmeier constants [5]. We used the Drude–Lorentz model to obtain the dielectric constant of the Au, and this model is characterized by the following equation [13]:

$$\varepsilon(\omega) = \varepsilon_1 + i\varepsilon_2 = \varepsilon_\infty - \frac{\omega_p^2}{\omega(\omega + \omega_c)}. \quad (2)$$

The meanings and values of ω_c, ω_p, and ω_∞ can be found in Ref. [13]. Moreover, the confinement loss (CL), which depends on the imaginary part of the effective RI (n_{eff}), can be found in the same reference.

The calculation was carried out by using COMSOL software. We imposed a circular anisotropic perfectly matched layer in order to absorb outgoing waves from the surface of the PCF. The complete meshed computation region consists of 37,010 elements, and the number of degrees of freedom equals 25,9703.

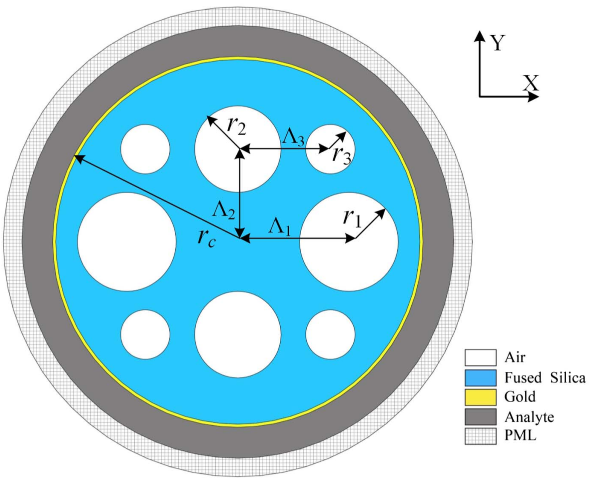

Fig. 1. Cross section of the proposed sensor.

3. SIMULATION RESULTS AND ANALYSIS

The performance of the SPR sensors depends on the geometrical parameters of the PCF. These parameters should be selected to make sure easy interaction between the evanescent field and the metal surface can be realized. The proposed sensor shows the birefringence due to asymmetric structure, which induces an effective index difference between the fundamental x polarization and y polarization modes as shown in Fig. 2.

Due to the highly birefringent structure, the confinement loss at y polarization resulted from higher SPR interaction, and the birefringence is much higher. As a result, the relevant modes at y polarization are used for analysis. Resonance occurs when the real part of the effective index of the fundamental mode matches with that of the plasmonic mode. Figure 3 shows the real part of the refractive index, the CL, and the field distribution of the fundamental and plasmonic modes as a function of wavelength. As can be seen from Fig. 3, the resonance occurs at a wavelength of 904 nm where the CL is maximum. Insets (a)–(c) illustrate the energy transition process between the fundamental mode and the plasmonic mode. It can be clearly observed that the two modes are different at non-resonant wavelengths [see insets (a) and (b)]. However, at the resonant wavelength, the real parts of the refractive indices of the fundamental mode and the plasmonic mode are identical (see the crossing point of red solid and dashed lines). The two modes become mixed [see inset (c)], which indicates that a portion of the fundamental mode energy couples into the plasmonic mode, leading to an obvious peak in the loss spectrum of the fundamental mode. In other words, the variation of n_a can be detected by measuring the shift of y-polarized resonance peak.

The influence of the hole size r_3 on the sensing performance is shown in Fig. 4. It can be seen that the plasmonic resonant loss increases when r_3 decreases. It is easy to understand, in that the decrease of the hole size in the outer layer promotes the leakage of the fundamental mode from the fiber core. This ultimately leads to the enhanced coupling between the fundamental mode and the plasmonic mode. Moreover, when r_3 decreases from 0.42 μm to 0.36 μm, the resonant peak redshifts from 901 nm to 910 nm, and the peak loss increases from

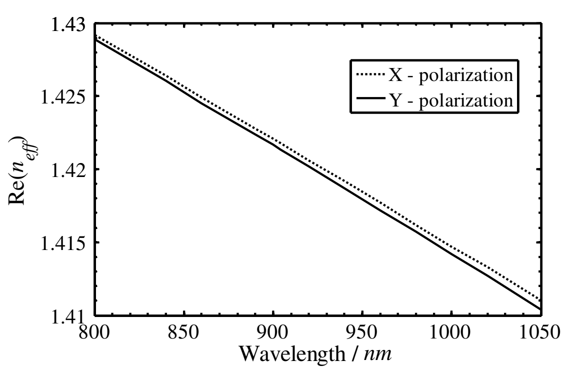

Fig. 2. Variation of effective indices of x and y polarizations showing birefringence behavior with $n_a = 1.40$, $\Lambda_1 = 1.8$ μm, $\Lambda_2 = \Lambda_3 = 1.5$ μm, $r_1 = 0.8$ μm, $r_2 = 0.7$ μm, $r_3 = 0.4$ μm, $r_c = 3$ μm, $t_{Au} = 30$ nm, and $t_{anal} = 0.5$ μm.

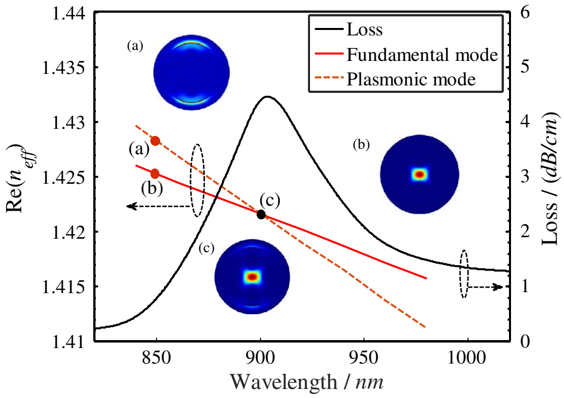

Fig. 3. Real part of the effective refractive index of the fundamental mode (red solid line) and the plasmonic mode (red dashed line), as well as the loss spectrum of the fundamental mode (black solid curve). Insets (a) and (b) show the electric field of plasmonic and fundamental modes at non-resonant wavelengths, respectively. Inset (c) shows the field distribution at resonant wavelength. The RI of analyte is 1.40. Structure parameters: $\Lambda_1 = 1.8$ μm, $\Lambda_2 = \Lambda_3 = 1.5$ μm, $r_1 = 0.8$ μm, $r_2 = 0.7$ μm, $r_3 = 0.4$ μm, $r_c = 3$ μm, $t_{Au} = 30$ nm, and $t_{anal} = 0.5$ μm.

3.2465 dB/cm to 8.2940 dB/cm, which indicates that r_3 has main effects on the resonance intensity of the sensor.

The asymmetrical structure caused by the different hole sizes leads to the birefringence. The greater the difference of hole size, the stronger the birefringence that will be induced. In order to investigate the effects of r_1 and r_2 on the birefringence, the variable $\delta = r_2/r_1$ is introduced. Figure 5 shows the loss spectrum for different δ with $n_a = 1.40$, $\Lambda_1 = 1.8$ μm, $\Lambda_2 = \Lambda_3 = 1.5$ μm, $r_c = 3$ μm, $t_{Au} = 30$ nm, and $t_{anal} = 0.5$ μm. It can be seen that the CL at the resonant wavelength increases, and the resonant wavelength moves toward the shorter wavelength (blue-shifted) with decreasing δ. It can be understood, in that smaller δ means stronger asymmetry and high birefringence, weakening the limitation of the optical field and increasing the leakage loss.

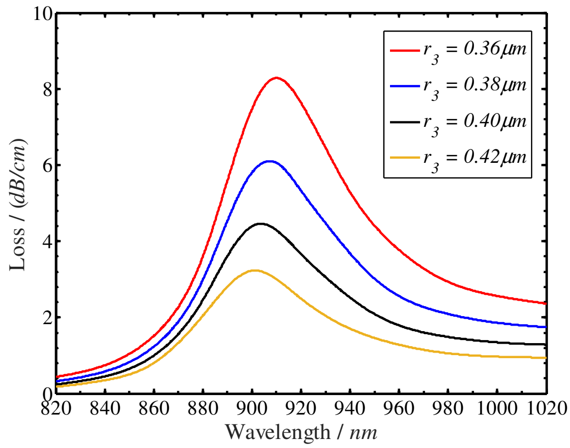

Fig. 4. Loss spectra of the sensor for different hole sizes r_3 with $n_a = 1.40$, $\Lambda_1 = 1.8$ μm, $\Lambda_2 = \Lambda_3 = 1.5$ μm, $r_1 = 0.8$ μm, $r_2 = 0.7$ μm, $r_c = 3$ μm, $t_{Au} = 30$ nm, and $t_{anal} = 0.5$ μm.

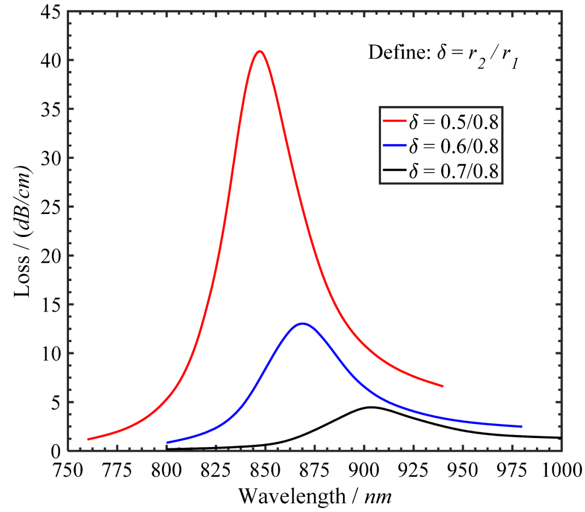

Fig. 5. Loss spectrum for different $\delta = r_2/r_1$ with $n_a = 1.40$, $\Lambda_1 = 1.8$ μm, $\Lambda_2 = \Lambda_3 = 1.5$ μm, $r_c = 3$ μm, $t_{Au} = 30$ nm, and $t_{anal} = 0.5$ μm.

The performance of the PCF-based SPR sensor can be measured by the sensitivity. We analyzed the sensitivity of the proposed fiber by using wavelength interrogation and amplitude interrogation. The wavelength sensitivity can be calculated as follows [13]:

$$S(\lambda) = \frac{\Delta\lambda_{peak}}{\Delta n_a} \text{ (nm/RIU)}, \tag{3}$$

where $\Delta\lambda_{peak}$ is the resonant wavelength shift, and Δn_a is the variation of the analyte RI. Figure 6 presents the peak wavelength shift by varying the external analyte RI from 1.40 to 1.43. The real part of the effective index Re(n_{eff}) of the plasmonic mode changes with the analyte RI, resulting in a red shift of the resonant wavelength [11]. It can be concluded that a positive wavelength sensitivity as high as 15180 nm/RIU can be achieved. From Fig. 7, it can be obtained that the linear regression R^2 of the resonant wavelength shift is as high as

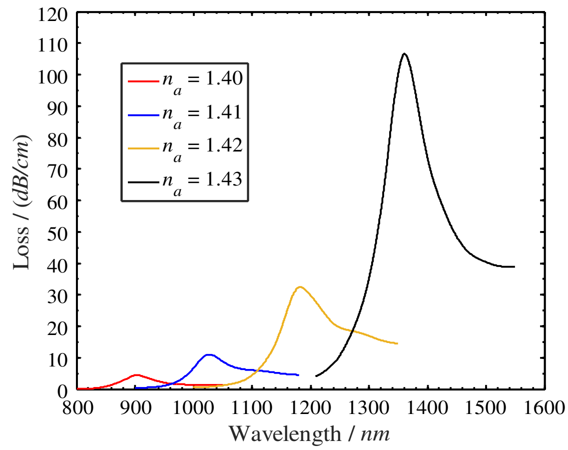

Fig. 6. Peak wavelength shifts of the sensor for different analyte RIs with parameters: $\Lambda_1 = 1.8$ μm, $\Lambda_2 = \Lambda_3 = 1.5$ μm, $r_1 = 0.8$ μm, $r_2 = 0.7$ μm, $r_3 = 0.4$ μm, $r_c = 3$ μm, $t_{Au} = 30$ nm, and $t_{anal} = 0.5$ μm.

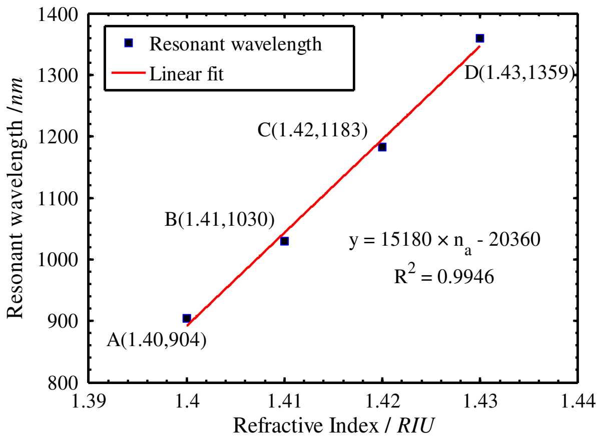

Fig. 7. Linear fitting of the resonant wavelength as a function of analyte RI for $\Lambda_1 = 1.8\ \mu\text{m}$, $\Lambda_2 = \Lambda_3 = 1.5\ \mu\text{m}$, $r_1 = 0.8\ \mu\text{m}$, $r_2 = 0.7\ \mu\text{m}$, $r_3 = 0.4\ \mu\text{m}$, $r_c = 3\ \mu\text{m}$, $t_{\text{Au}} = 30$ nm, and $t_{\text{anal}} = 0.5\ \mu\text{m}$.

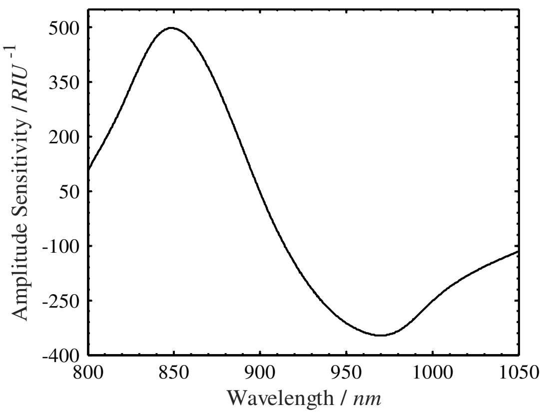

Fig. 8. Amplitude sensitivity of the sensor with optimized parameters $\Lambda_1 = 1.8\ \mu\text{m}$, $\Lambda_2 = \Lambda_3 = 1.5\ \mu\text{m}$, $r_1 = 0.8\ \mu\text{m}$, $r_2 = 0.7\ \mu\text{m}$, $r_3 = 0.4\ \mu\text{m}$, $r_c = 3\ \mu\text{m}$, $t_{\text{Au}} = 30$ nm, and $t_{\text{anal}} = 0.5\ \mu\text{m}$.

0.9946 with the iteration of 0.01, showing a very high linearity and providing the ability of accurate analyte detection.

The amplitude sensitivity of the PCF-SPR sensor is analyzed and can be calculated as [5]

$$S\ (\text{RIU}^{-1}) = -\frac{1}{\alpha(\lambda, n_a)} \frac{\partial\alpha(\lambda, n_a)}{\partial n_a}, \tag{4}$$

where $\alpha(\lambda, n_a)$ is the transmission loss corresponding to n_a, and $\partial\alpha(\lambda, n_a)$ is the loss difference between two loss spectra [14]. Figure 8 shows that the amplitude sensitivity varies with the wavelength at a refractive index of 1.40. The amplitude sensitivity increases first and then decreases with increasing wavelength, and S_A can reach up to 498 RIU^{-1}.

4. CONCLUSIONS

We propose a highly sensitive and simple SPR-PCF sensor to achieve accurate sensing. Both thin Au film and analyte are at the outer surface of the PCF, ensuring easy fabrication and more practical detection. The asymmetric structure provides the sensor with high birefringence to enable high sensitivity. Compared with existing multi-coating and inner-coating configurations, our sensor is much simpler and more sensitive. Besides the high linearity, the wavelength sensitivity of the sensor is found to be as high as 15180 nm/RIU, the amplitude sensitivity is up to 498 RIU^{-1}, and the resolution of the sensor can be 5.6818×10^{-6} RIU, which is very competitive in biochemical and biological analyte detection.

Funding. National Natural Science Foundation of China (NSFC) (61475029).

Acknowledgment. We thank the Key Laboratory of Optoelectronic Technology and Systems (Education Ministry of China) for the use of its equipment.

REFERENCES

1. X. Yu, Y. Zhang, S. Pan, P. Shum, M. Yan, Y. Leviatan, and C. Li, "A selectively coated photonic crystal fiber based surface plasmon resonance sensor," J. Opt. **12**, 015005 (2010).
2. B. Shuai, L. Xia, Y. Zhang, and D. Liu, "A multi-core holey fiber based plasmonic sensor with large detection range and high linearity," Opt. Express **20**, 5974–5986 (2012).
3. Y. Peng, J. Hou, Z. Huang, and Q. Lu, "Temperature sensor based on surface plasmon resonance within selectively coated photonic crystal fiber," Appl. Opt. **51**, 6361–6367 (2012).
4. G. An, S. Li, W. Qin, W. Zhang, Z. Fan, and Y. Bao, "High-sensitivity refractive index sensor based on D-shaped photonic crystal fiber with rectangular lattice and nanoscale gold film," Plasmonics **9**, 1355–1360 (2014).
5. M. R. Hasan, S. Akter, A. A. Rifat, S. Rana, and S. Ali, "A highly sensitive gold-coated photonic crystal fiber biosensor based on surface plasmon resonance," Photonics **4**, 18 (2017).
6. W. Qin, S. Li, Y. Yao, X. Xin, and J. Xue, "Analyte-filled core self-calibration microstructured optical fiber based plasmonic sensor for detecting high refractive index aqueous analyte," Opt. Lasers Eng. **58**, 1–8 (2014).
7. X. Yang, Y. Lu, B. Liu, and J. Yao, "Analysis of graphene-based photonic crystal fiber sensor using birefringence and surface plasmon resonance," Plasmonics **12**, 489 (2016).
8. A. A. Rifat, G. A. Mahdiraji, D. M. Chow, Y. G. Shee, R. Ahmed, and F. R. M. Adikan, "Photonic crystal fiber-based surface plasmon resonance sensor with selective analyte channels and graphene-silver deposited core," Sensors **15**, 11499–11510 (2015).
9. Z. Fan, S. Li, Q. Liu, G. An, H. Chen, J. Li, D. Chao, H. Li, J. Zi, and W. Tian, "High sensitivity of refractive index sensor based on analyte-filled photonic crystal fiber with surface plasmon resonance," IEEE Photon. J. **7**, 1–9 (2015).
10. D. Li, W. Zhang, H. Liu, J. Hu, and G. Zhou, "High sensitivity refractive index sensor based on multicoating photonic crystal fiber with surface plasmon resonance at near-infrared wavelength," IEEE Photon. J. **9**, 6801608 (2017).
11. N. Luan and J. Yao, "Refractive index and temperature sensing based on surface palsmon resonance and directional resonance coupling in a PCF," IEEE Photon. J. **9**, 6801307 (2017).
12. C. Liu, L. Yang, W. Su, F. Wang, T. Sun, Q. Liu, H. Mu, and P. K. Chu, "Numerical analysis of a photonic crystal fiber based on a surface plasmon resonance sensor with an annular analyte channel," Opt. Commun. **382**, 162–166 (2017).
13. M. Liu, X. Yang, B. Zhao, J. Hou, and P. Shum, "Square array photonic crystal fiber based surface plasmon resonance refractive index sensor," Mod. Phys. Lett. B **31**, 1750352 (2017).
14. C. Liu, L. Yang, Q. Liu, F. Wang, Z. Sun, T. Sun, H. Mu, and P. K. Chu, "Analysis of a surface plasmon resonance probe based on photonic crystal fibers for low refractive index detection," Plasmonics **10**, 1–6 (2017).